Correspondence

Analysis of the Optimum Configuration of Roadside Units and Onboard Units in Dedicated Short-Range Communication Systems

Wern-Yarng Shieh, Wei-Hsun Lee, Shen-Lung Tung, Bor-Shenn Jeng, and Cheng-Hsin Liu

***Abstract*—With the aid of a simple relation, which is analogous to the radar equation, the uplink signal strength received by the receiving module of a roadside unit (RSU) and emitted from the radiation module of an onboard unit (OBU) can be described. Setting the scale of this relation arbitrarily and determining the signal strength threshold from experimental measurements, and combined with the simulation of the radiation and the receiving pattern by $\cos ine^n$ function, the relative signal strength emitted from the OBU and received by the RSU can be calculated successfully. From this computed relative signal strength and the threshold, the influence of the RSU and OBU mounting parameters, such as the mounting angles and mounting height, on the available communication region is analyzed. The effect of windshield fading is also considered. With the help of the analysis results, an optimum RSU and OBU mounting configuration can be easily obtained. This method can be used conveniently and successfully for very short wavelengths. This includes visible light, infrared, and even submillimeter-wave ranges. For millimeter-wave and microwave systems, this method can, in some cases, also provide a rudimentary estimation.**

***Index Terms*—Dedicated short-range communication (DSRC), electronic toll collection (ETC), infrared communication, intelligent transportation system (ITS).**

I. Introduction

In many intelligent transportation systems (ITSs), in particular electronic toll collection (ETC) systems, a sufficient period of time is necessary to allow for the complete transfer of all the data between a roadside unit (RSU) and an onboard unit (OBU) while vehicles are rapidly travelling through the communication region. The mounting configuration of the RSU and the OBU can affect both uplink and downlink data transmission in dedicated short-range communication systems (DSRCs). Hence, the mounting angles of both RSU and OBU as well as the RSU mounting height should be carefully determined for optimum communications. This will allow for an extended region of communication. The arrangement of RSU and OBU is important not only for single-lane but also for multilane free-flow systems. This is because, in general, the communication regions for contiguous traffic lanes of the latter are overlapping [1], and this needs to be carefully considered. Apart from ETC, there are other ITS short-range communication applications in which the configuration of transmitter and receiver setup is also important for the performance of data transmission [2]–[4]. Therefore, there is a need for a detailed analysis of the optimum mounting configuration for RSU and OBU. Thus, an easy-to-use theoretical method may be beneficial.

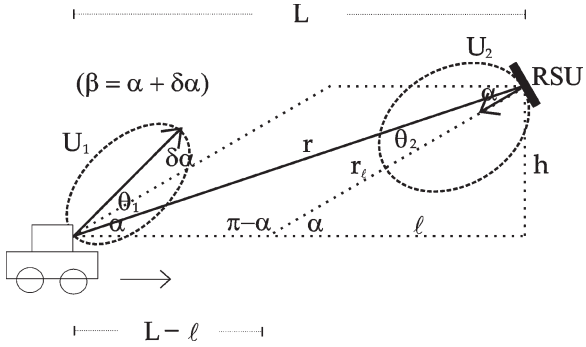

Fig. 1. Single-lane RSU and OBU mounting configuration.

Recently, Visser *et al.* suggested a physical model to estimate the reliability of the microwave DSRC link for ETC applications [5], in which the received signal strength was obtained by calculating the antenna pattern. Here, we introduce an easy-to-implement and precise method to estimate the available communication region of short-range communication systems. Our method is based on a simple relation analogous to the radar equation, i.e., the expression of the received signal strength of communication between the OBU and the RSU. Most importantly, the signal strength threshold is determined experimentally. The proposed method was successfully tested in an infrared short-range communication system. It is expected that the present method will be widely applicable, in particular, for very short wavelengths such as visible light and even in the submillimeter-wave range. Incidentally, there have been several ITS applications that utilize traffic lights as a communication tool [2], [3]. Such systems can also be analyzed by the method suggested in this paper.

In this paper, we describe the numerical results in one-dimensional (1-D), i.e., single-lane, case. The two-dimensional (2-D) results will be presented in a subsequent paper.

II. Signal Strength Relation

To estimate the available communication region of a certain RSU and OBU setup, it is desirable to determine if the data transmission is successful. In DSRC systems, the radiation power of an RSU is generally stronger than that of an OBU so that the downlink communication region is wider than that of the uplink. Hence, it is the capability of the uplink communication that is crucial for data transmission. Therefore, we will focus only on the uplink transmission in the following discussions. The calculation of downlink data transmission may follow in a similar manner.

A. Mounting Configuration of RSU and OBU

The signal strength received by the RSU from the emission of OBU depends on the radiation power and pattern of OBU, the receptivity and the receiving pattern of RSU, and the relative location and direction

Manuscript received May 10, 2004; revised September 15, 2004, June 7, 2005, January 10, 2006, and June 22, 2006. This work was supported by the Project of Intelligent Transportation Systems at the Research Institute of ChungHwa Telecom (former ChungHwa Telecommunication Laboratories). The Associate Editor for this paper was C. K. Toh.

W.-Y. Shieh is with the Department of Electronic Engineering, St. John's University, Taipei 25135, Taiwan, R.O.C. (e-mail: shiehwy@mail.sju.edu.tw).

W.-H. Lee is with the Research Institute of Chunghwa Telecom, Taoyuan 326, Taiwan, R.O.C., and also with the Department of Computer Science, National Chiao Tung University, Hsinchu 300, Taiwan, R.O.C. (e-mail: leews@cht.com.tw).

S.-L. Tung and B.-S. Jeng are with the Research Institute of Chunghwa Telecom, Taoyuan 326, Taiwan, R.O.C. (e-mail: tung168@cht.com.tw; bsjip@cht.com.tw).

C.-H. Liu is with Chung Shan Institute of Science and Technology, Taoyuan 325, Taiwan, R.O.C. (e-mail: james_masa@yahoo.com.tw).

Digital Object Identifier 10.1109/TITS.2006.884888

between OBU and RSU. Fig. 1 shows a single-lane RSU and OBU mounting configuration. The RSU is mounted at a vertical height h above the horizontal plane of the OBU with a declination angle α relative to the horizontal plane. The OBU is mounted with an upward angle β relative to the horizontal plane, where $\beta = \alpha + \delta\alpha$. The distance between OBU and RSU is

$$r = (L^2 + h^2)^{\frac{1}{2}} \tag{1}$$

and the values of θ_1 and θ_2 can be obtained from

$$\cos\theta_2 = \frac{r^2 + r_l^2 - (L-l)^2}{2rr_l} \tag{2}$$

and

$$\theta_1 = \theta_2 + \delta\alpha \tag{3}$$

where θ_1 and θ_2 are the angles between the data transmission line (line r in Fig. 1) and the direction of the OBU and RSU, respectively. The directions of the OBU and RSU are marked by arrows in Fig. 1. In (2), we also need

$$l = \frac{h}{\tan\alpha}$$

and

$$r_l = \frac{h}{\sin\alpha}.$$

B. Signal Strength Received by RSU

The signal strength S emitted from the OBU and received by the RSU may be expressed by an expression analogous to the widely used radar equation [6], [7]

$$S = \frac{P_o}{4\pi r^2} U_1(\theta_1, \phi_1) A_e U_2(\theta_2, \phi_2) \tag{4}$$

where P_o denotes the total emitting power of the radiation module of the OBU, r is the distance between the OBU and the RSU, A_e is the area of the effective receiving aperture of the receiving module of the RSU, $U_1(\theta_1, \phi_1)$ is the radiation pattern of the OBU, and $U_2(\theta_2, \phi_2)$ is the receiving pattern of the RSU. U_1 and U_2 are functions of emitting direction (θ_1, ϕ_1) and receiving direction (θ_2, ϕ_2), respectively, where θ_1, ϕ_1, θ_2, and ϕ_2 are defined following the conventional polar coordinates shown in Fig. 1. (Note that ϕ_1 and ϕ_2 are not displayed in this 2-D figure.) Equation (4) can be simplified as

$$S = A_0 \frac{U_1(\theta_1, \phi_1) U_2(\theta_2, \phi_2)}{r^2} \tag{5}$$

where A_0 is the amplitude constant of the received signal strength, which is determined by the emitting power of the OBU, the receiving capability of the RSU, and the fading caused by absorption and reflection of the transmission media (air, windshield, etc.). The formulation and numerical values of U_1, U_2, and A_0 are discussed as follows.

1) Radiation Pattern of OBU: The radiation pattern of an emitting module can be simulated by the $\cos^n$ function, which has been widely used for infrared sources [8]–[10] as well as in antenna pattern analysis [11]. Here, we show an example.

The infrared radiation module of an OBU was composed of several Vishay Telefunken TSHF5400 high-speed infrared light-emitting diodes (LED) with wavelength of 870 nm and half-intensity angle of 22°. Related data on this diode can be found in the manufacturer's datasheet [12]. Since the LED light is incoherent, and the LED module (< 3 cm) is very small compared with the distance r (a few meters) between the OBU and the RSU, the LED module can be treated as a point source. The radiation pattern of this LED module was measured. We found that its half-intensity angle $\phi_{(1/2)}$ was around 24°. The measured radiation pattern is shown in Fig. 2 in (a) polar coordinates and (b) rectangular coordinates. A function of $\cos^{7.5}$ was chosen to simulate this radiation pattern, i.e.,

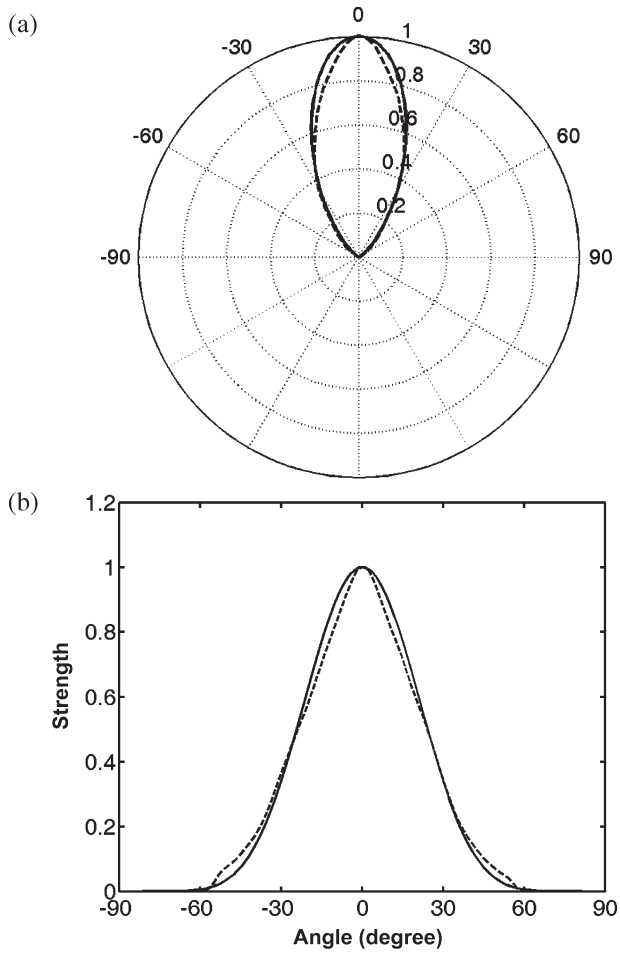

Fig. 2. Comparison of the result of measurement of the radiation pattern of the infrared radiation module (dashed line) with that simulated by $\cos^{7.5}\theta$ (solid line) in (a) polar coordinates and (b) rectangular coordinates. Both results have a half-intensity angle $\phi_{(1/2)} = 24°$.

$$U_1 = \cos^{7.5}\theta_1 \tag{6}$$

where θ_1 is defined as in Fig. 1. This simulation is also plotted in Fig. 2 (solid line) to compare with the measured results, and it shows reasonable agreement with these measurements. The simulation of radiation pattern by a simple function allows for easy implementation in the computation programs.

2) Receiving Pattern of RSU: The receiving module of an RSU was composed of several OSRAM BPW34 PIN photodiodes. Related data on this diode can be found in the manufacturer's datasheet [13]. Since the data communication wavelength of 870 nm is far shorter than the dimension (a few millimeters) of the receiving photodiodes, the receiving cross section of the photodiodes can be obtained by simple

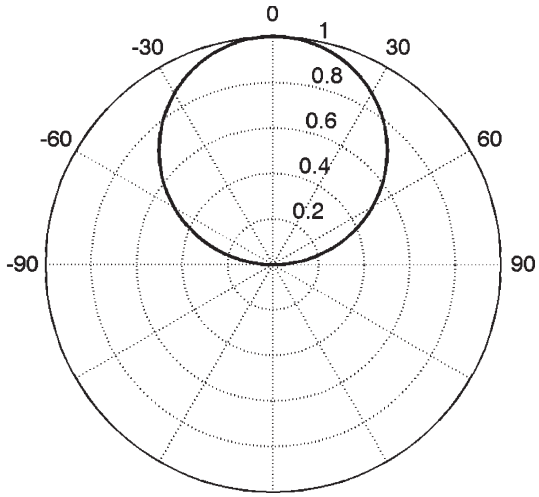

Fig. 3. Receiving pattern $(\cos\theta)$ of the photodiode receiving module of the RSU.

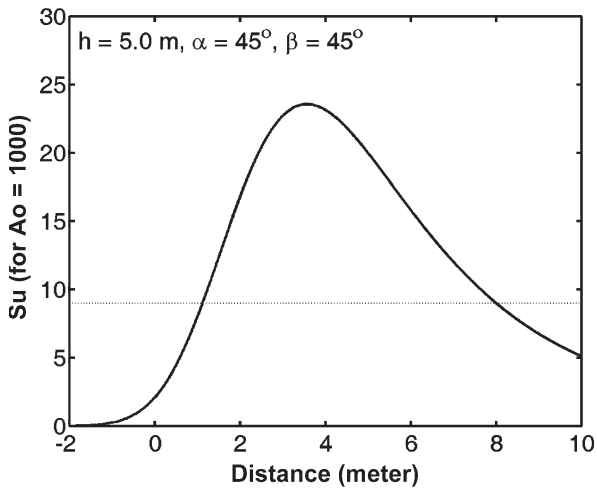

Fig. 4. Relative signal strength (S_u, solid line) received by the RSU and emitted from the OBU for $h = 5.0$ m, $\alpha = 45°$, and $\beta = 45°$, arbitrarily setting $A_0 = 1000$. The horizontal dotted line indicates the signal strength threshold $S_{\rm th}$.

geometrical optics. Therefore, the receiving pattern of the photodiodes module can be simply written as

$$U_2 = \cos\theta_2 \tag{7}$$

where θ_2 is defined as in Fig. 1. Fig. 3 shows the receiving pattern of (7).

III. Numerical Results

Substituting (6) and (7) into (5), we obtain

$$S = A_0 \frac{\cos^{7.5}\theta_1 \cos\theta_2}{r^2}. \tag{8}$$

Equation (8) denotes the signal strength emitted from the OBU and received by the RSU under single-lane, i.e., 1-D, conditions. Now, the difficulty arises: We cannot obtain the value of the amplitude constant A_0 unless we know the details of all the complicated factors such as the total power emission from the OBU, the receptivity of the RSU, and the fading due to the absorption and reflection of the transmission media. This is not an easy task. To overcome this, we have adopted a convenient approach with the aid of a simple experimental measurement, as discussed in the next subsection.

A. Determination of the Amplitude Constant A_0 and the Signal Strength Threshold $S_{\rm th}$

A successful communication requires that the received signal strength S be greater than the threshold $S_{\rm th}$ of the communication system, i.e., $S > S_{\rm th}$. For a certain communication system, the ratio of the threshold $S_{\rm th}$ to the amplitude constant A_0 is a constant that is independent of the scale, i.e.,

$$\frac{S_{\rm th}}{A_0} = \text{constant}.$$

This ratio is affected only by background noise level and is larger for higher background noise and smaller for lower background noise. For our purposes, the scale in (8) is not important. Hence, we are only concerned with the relative magnitude of S. This means we can arbitrarily choose a scale in (8).

Fig. 4 shows the calculated relative signal strength (solid line) for A_0 arbitrarily chosen as $A_0 = 1000$, i.e.,

$$S_u = 1000 \frac{\cos^{7.5}\theta_1 \cos\theta_2}{r^2} \tag{9}$$

TABLE I
Calculated Results of S_u for Values Near the Observed Communication Boundaries

L (meter)	S_u	S_u	L (meter)
8.43	7.957997	7.896740	0.98
8.42	7.980991	7.977856	0.99
8.41	8.004055	8.059314	1.00
8.40	8.027190	8.141107	1.01
8.39	8.050397	8.223232	1.02
8.38	8.073674	8.305681	1.03
8.37	8.097022	8.388451	1.04
·	·	8.471536	1.05
·	·	8.554930	1.06
·	·	8.638627	1.07
8.04	8.908542	8.722622	1.08
8.03	8.934407	8.806910	1.09
8.02	8.960349	8.891484	1.10
8.01	8.986367	8.976339	1.11
8.00	9.012463	9.061469	1.12
7.99	9.038635	9.146867	1.13
7.98	9.064885	9.232529	1.14

for the OBU travelling from 10.0 to -2.0 m and for a typical mounting configuration of $h = 5.0$ m and $\alpha = \beta = 45°$. [In the coordinates of our calculations, we set the RSU at $(0, h)$, and the OBU travels from (10.0 m, 0) to (-2.0 m, 0).]

From the measurements of an infrared short-range communication system, for the aforementioned mounting configuration $h = 5.0$ m and $\alpha = \beta = 45°$, we obtained an available communication region from $L = 8.0$ m to $L = 1.0$ m with an available communication length of 7.0 m. In Table I, we list some calculated results of S_u for values near the observed communication boundaries to help determine the threshold $S_{\rm th}$. For L at 8.0 and 1.0 m, the signal strength S_u can be read as 9.01 and 8.06, respectively. In the case of choosing $S_{\rm th} = 8.0$, we will obtain an available communication region between 1.0 and 8.41 m with an available communication length of 7.41 m. On the other hand, for $S_{\rm th} = 9.0$, the available communication region is from 8.0 to 1.12 m with a length of 6.88 m. In the present analysis, we prefer a more stringent criteria, i.e., $S_{\rm th} = 9.0$. This signal strength threshold level is indicated by the horizontal dotted line in Fig. 4.

The above definitions of A_0 and $S_{\rm th}$ have shown good agreement with the experimental measurements. With these two definitions, the signal strength relation can be established, and the analysis can be

performed with the aid of (9). For other systems with different emitting power, radiation pattern, receiving pattern, and/or responsivity, the procedure of analysis is the same.

Although an imprecise value of the threshold $S_{\rm th}$ may slightly affect the calculated available communication region (larger or smaller), it is not critical for finding an optimum configuration between RSU and OBU.

B. Influence of the Mounting Parameters on the Received Signal Strength and the Available Communication Region

The three most important mounting parameters that affect the received signal strength are the mounting height h, the declined angle α of the RSU, and the up-inclined angle β of the OBU. Also, the signal fading due to the windshield is important, and we will discuss all of these parameters separately in the following subsections.

1) Effects of the RSU Mounting Height: Fig. 5(a) shows the received signal strength for $\alpha = 45^\circ$, $\beta = 45^\circ$, and $h = 3, 4, 5,$ and 6 m, respectively. The difference in vertical height may correspond to OBUs mounted on different kinds of vehicles such as small cars, vans, trucks, . . ., etc. As shown in the figure, for increasing vertical height, the signal strength decreases, as expected. Fig. 5(b) shows the boundaries of the available communication region, where Lf_u denotes the far boundary, and Ln_u denotes the near boundary. In the region between Lf_u and Ln_u, the data transmission is successful. As shown in the figure, for increasing vertical height, the available communication region shifts slightly toward the approaching vehicle side. Fig. 5(c) shows the length of the available communication region $L_a (L_a = Lf_u - Ln_u)$ as a function of h. The value of L_a varies between 6.22 and 7.10 m with the maximum of 7.10 m occurring at $h = 4.0$ m.

2) Effects of the RSU Mounting Angle: Fig. 6(a) shows the received signal strength S_u for $h = 4$ m, $\beta = 45^\circ$, and $\alpha = 30^\circ,\ 45^\circ,\ 60^\circ$, respectively, where the peak value of the signal strength increases slightly with the increase of α. It can be seen that the available communication boundaries [Fig. 6(b)] and the available communication length [Fig. 6(c)] are not significantly affected by the RSU mounting angle. This is due to the wider receiving pattern (less directivity) of the receiving module of the RSU. The variation of L_a is not remarkable, which is between 6.87 and 7.12 m, while the maximum is located at $\alpha = 38^\circ$ with a value of 7.12 m. For the narrower radiation pattern (higher directivity) of the OBU (see Figs. 2 and 3), the influence of its mounting angle is more significant for the uplink data transmission, and it will be discussed in the following subsection.

3) Effects of the OBU Mounting Angle: Fig. 7(a) shows the received signal strength S_u for $h = 4$ m, $\alpha = 45^\circ$, and $\beta = 30^\circ, 45^\circ,$ and 60°. The peak value of S_u increases with the increase of β, and the available communication region recedes toward the direction of the RSU as shown in Fig. 7(b). The variation of L_a is between 6.19 and 7.46 m, with the maximum of 7.46 m occurring at $\beta = 33^\circ$ [Fig. 7(c)]. The different β may correspond to the setup of OBU by users with different mounting angles. As can be seen, for the uplink data transmission, the signal strength and the range of the communication region are more sensitive to the mounting angle of OBU than that of RSU.

4) Effects of Fading on the Received Signal Strength: The received signal strength may be suppressed due to the fading effect of the vehicle windshields and bad weather conditions such as rain or fog. In the present analysis, this effect was taken into account by a fading factor f_a multiplied to (5), i.e.,

$$S = A_0 f_a \frac{U_1(\theta_1, \phi_1) U_2(\theta_2, \phi_2)}{r^2}. \tag{10}$$

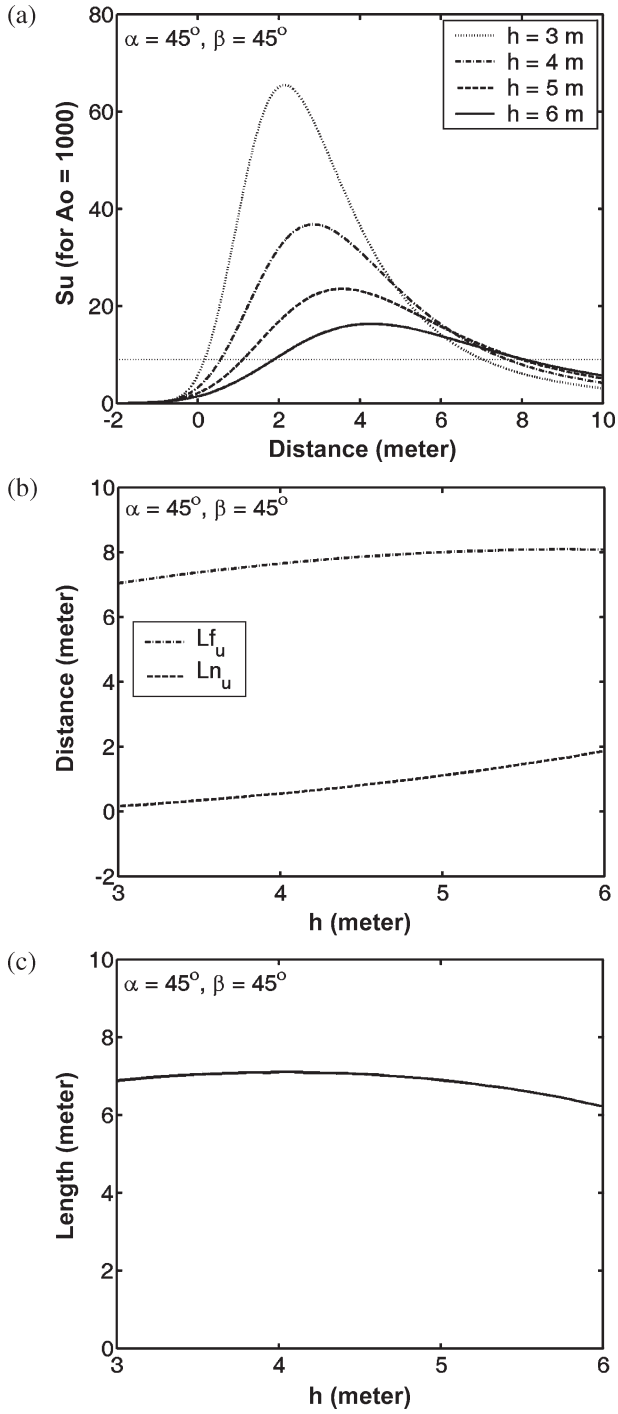

Fig. 5. (a) Received signal strength for $\alpha = 45^\circ$, $\beta = 45^\circ$, and $h = 3, 4, 5,$ and 6 m. The horizontal dotted line indicates the signal strength threshold. (b) Boundaries of the available communication region as a function of h. (c) Available communication length L_a as a function of h. Both (b) and (c) are for $\alpha = 45^\circ$ and $\beta = 45^\circ$.

The value of f_a can be obtained experimentally, and measurement for various kinds of commercial windshields showed that the transmissivity for 870-nm infrared light varied from 0.8 to 0.15.

Fig. 8(a) shows the received signal strength S_u for $h = 4$ m, $\alpha = \beta = 45^\circ$, and $f_a = 1.0,\ 0.8,\ 0.6,$ and 0.4, respectively, which correspond to 0%, 20%, 40%, and 60% fading of the signal. As expected, the received signal strength decreases with increasing fading, and the available communication region reduces accordingly, as shown in Fig. 8(b) and (c).

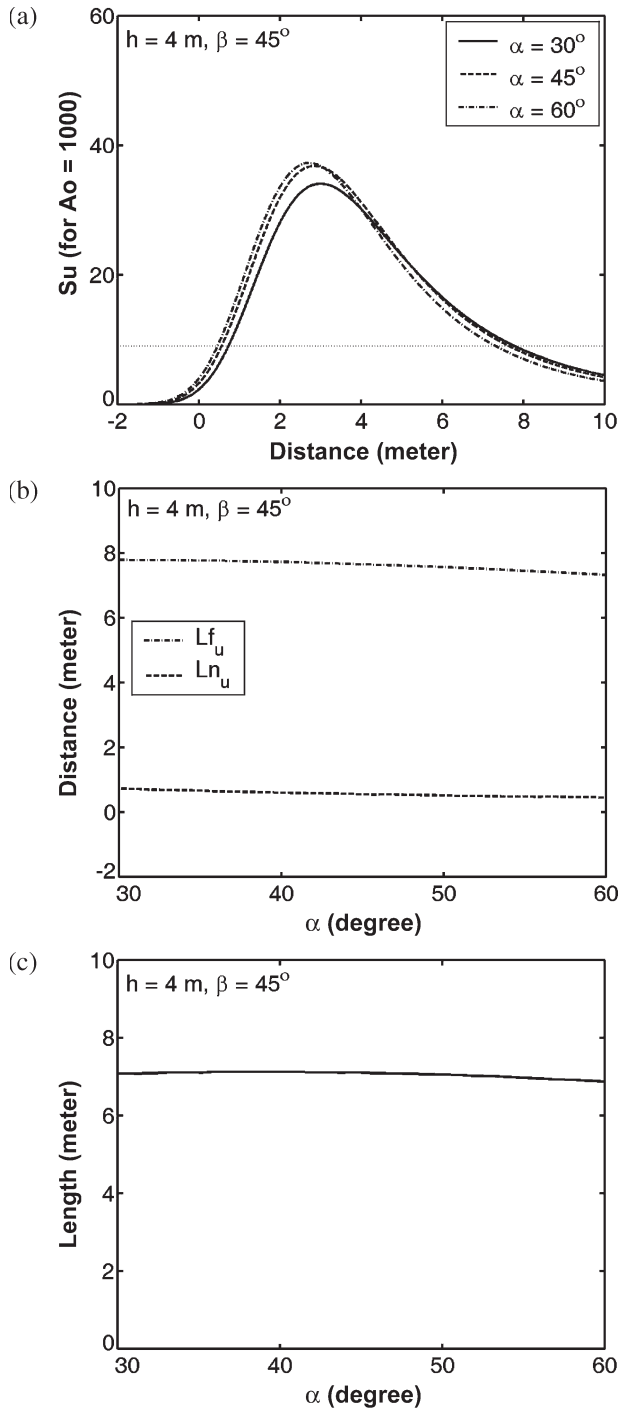

Fig. 6. (a) Received signal strength for $h = 4$ m, $\beta = 45°$, and $\alpha = 30°, 45°$, and $60°$. The horizontal dotted line indicates the signal strength threshold. (b) Boundaries of the available communication region as a function of α. (c) Available communication length L_a as a function of α. Both (b) and (c) are for $h = 4$ m and $\beta = 45°$.

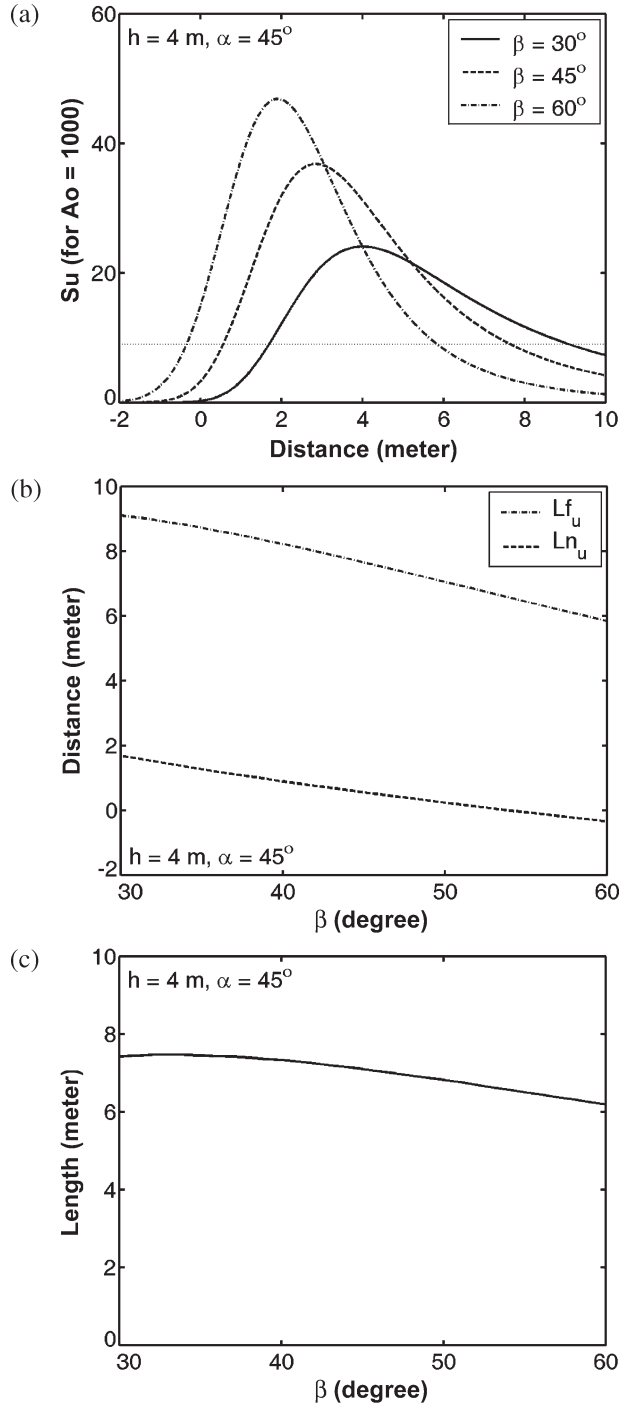

Fig. 7. (a) Received signal strength for $h = 4$ m, $\alpha = 45°$, and $\beta = 30°, 45°$, and $60°$. The horizontal dotted line indicates the signal strength threshold. (b) Boundaries of the available communication region as a function of β. (c) Available communication length L_a as a function of β. Both (b) and (c) are for $h = 4$ m and $\alpha = 45°$.

IV. Optimum Configuration

The optimum configuration in a DSRC system was expected to be the one with the longest available communication length L_a under conditions of pronounced signal fading due to windshield or weather. The parameters that affect this optimum configuration include the mounting height of the RSU and the mounting angles of the RSU and OBU. For fixed RSU and OBU mounting angles, the uplink received signal strength is higher for lower RSU mounting height. This is due to the $1/r^2$ factor in the signal strength equation [see (5), (9), and Fig. 5]. Unfortunately, in order to conform to the height of larger trucks, the RSU mounting height generally cannot be lower than 5.5 m above the ground. This leads to the fact that the value of h was limited between 4.5 m (for small cars) and 3.5 m (for larger trucks). Therefore, the remaining adjustable parameters are the mounting angles of the RSU and OBU.

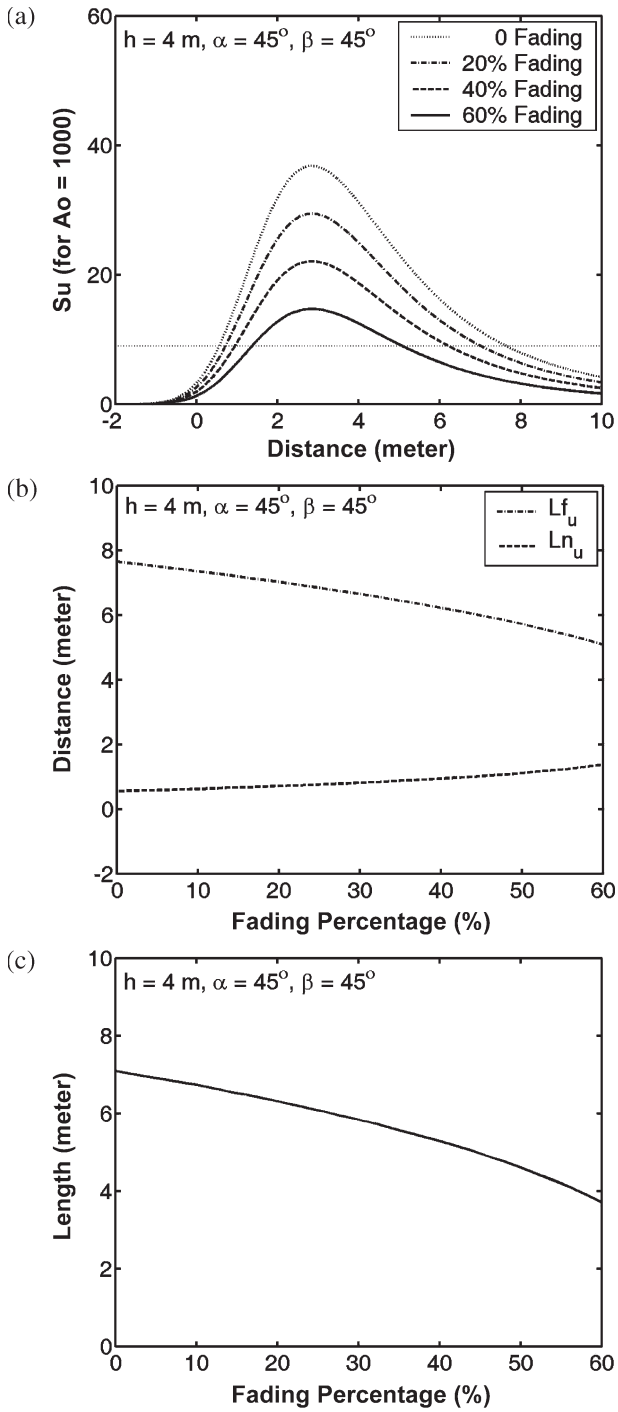

Fig. 8. (a) Received signal strength for different fading for $h = 4$ m, $\alpha = 45^\circ$, and $\beta = 45^\circ$. The horizontal dotted line indicates the signal strength threshold. (b) Boundaries of the available communication region as a function of fading percentage. (c) Available communication length L_a as a function of fading percentage. Both (b) and (c) are for $h = 4$ m, $\alpha = 45^\circ$, and $\beta = 45^\circ$.

For uplink data transmission, the signal strength is more sensitive to the mounting angle of OBU than that of RSU due to the difference between the directivities of the corresponding radiation pattern and receiving pattern [Figs. 2(a) and 3]. From the analysis in Section III, without considering the fading effects, it is natural to choose α near 38° and β near 33° to obtain the longest available communication length. However, for small mounting angles $(\alpha, \beta < 45^\circ)$, the peak value of the signal strength is relatively low, which may cause a severe shrinkage of available communication region when fading exists. This can be easily understood by an inspection of Fig. 7(a), where $h = 4$ m, $\alpha = 45^\circ$, the peak values of the received signals for $\beta = 30^\circ$ and 60° are 24.095 and 46.897, respectively. For low fading, say $f_a = 0.7$ (30% fading), the available communication lengths (L_a) were 5.54 m $(\beta = 30^\circ)$ and 5.30 m $(\beta = 60^\circ)$, respectively. But for high fading, for example, for $f_a = 0.3$ (70% fading), the available communication lengths became 0 for $\beta = 30^\circ$ and 2.89 m for $\beta = 60^\circ$. This means that under the condition of $h = 4$ m, $\alpha = 45^\circ$, and 70% fading, for $\beta = 30^\circ$, the system will not be able to provide successful communication. On the other hand, for the condition of $\beta = 60^\circ$, the system can still provide successful communication with a communication length of 2.89 m. Experiments confirmed that some windshields can cause 80% fading $(f_a = 0.2)$ for 870-nm infrared. Hence, fading has a significant effect on an infrared DSRC system.

To avoid severe reduction of the available communication region due to high fading, larger mounting angles of both RSU and OBU $(\alpha, \beta > 45^\circ)$ are recommended to maintain higher signal strength. Therefore, a compromised optimum configuration to avoid the severe influence of high fading for an infrared short-range communication system in ETC applications can be produced with $45^\circ < \alpha, \beta < 60^\circ$, and with the RSU vertical mounting height limited to its minimum value of 5.5 m relative to the ground.

V. Conclusion

In DSRC systems for ETC applications, a sufficient communication region is required to allow successful data transmission between RSU and OBU. To fulfill this requirement, an understanding of the influence of the mounting parameters of the OBU and RSU as well as the effects of signal fading is helpful. The important parameters include the OBU and RSU mounting angles and the vertical height of the RSU. Additionally, another critical factor is the power fading of windshields.

Using (5) with an arbitrary scale, i.e., arbitrarily setting a value to the amplitude constant A_0, together with a method to experimentally determine the signal strength threshold, the received signal strength relation can be established. With the aid of the $\cos^n$ function (or other suitable functions), the radiation and the receiving pattern of OBU and RSU can be simulated. Thus, the effects of the mounting parameters and fading can be analyzed, and the optimum mounting configuration can be obtained successfully from the analysis.

For smaller mounting angles $(30^\circ < \alpha, \beta < 45^\circ)$, the available communication region is greater than that of larger mounting angles $(45^\circ < \alpha, \beta < 60^\circ)$ under low-fading conditions. However, the available communication region is significantly reduced under the circumstances of high fading. To maintain sufficient size of the available communication region, a higher peak value of the received signal strength is required, which can be obtained by larger mounting angles $(45^\circ < \alpha, \beta < 60^\circ)$ of the OBU and RSU. Under the restriction of the minimum RSU mounting height of 5.5 m (relative to the ground) in order to conform to the height of large trucks, we obtain an optimum configuration $45^\circ < \alpha, \beta < 60^\circ$ for an infrared short-range communication system in ETC applications.

Although we have used a typical example to demonstrate the method for an infrared short-range communication system, this method is also widely applicable for very short wavelengths such as visible light and even in the submillimeter-wave range. For millimeter-wave and microwave bands, it is believed that the present method can still provide a rudimentary estimation in some cases.

Acknowledgment

The authors would like to thank the assistance by colleagues participating in this paper.

REFERENCES

[1] W.-Y. Shieh, W.-H. Lee, S.-L. Tung, and C.-D. Ho, "A novel architecture for multilane-free-flow electronic-toll-collection systems in the millimeter-wave range," *IEEE Trans. Intell. Transp. Syst.*, vol. 6, no. 3, pp. 294–301, Sep. 2005.

[2] G. K. H. Pang and H. H. S. Liu, "LED location beacon system based on processing of digital images," *IEEE Trans. Intell. Transp. Syst.*, vol. 2, no. 3, pp. 135–150, Sep. 2001.

[3] M. Akanegawa, Y. Tanaka, and M. Nakagawa, "Basic study on traffic information system using LED traffic lights," *IEEE Trans. Intell. Transp. Syst.*, vol. 2, no. 4, pp. 197–203, Dec. 2001.

[4] J. S. Kwak and J. H. Lee, "Infrared transmission for intervehicle ranging and vehicle-to-roadside communication systems using spread-spectrum technique," *IEEE Trans. Intell. Transp. Syst.*, vol. 5, no. 1, pp. 12–19, Mar. 2004.

[5] A. Visser, H. H. Yakah, A. J. van der Wees, M. Oud, G. A. van der Spek, and L. O. Herzberger, "A hierarchical view on modeling the reliability of a DSRC link for ETC applications," *IEEE Trans. Intell. Transp. Syst.*, vol. 3, no. 2, pp. 120–129, Jun. 2002.

[6] B. Edde, *Radar—Principles, Technology, Applications*. Englewood Cliffs, NJ: Prentice-Hall, 1993, ch. 1.

[7] M. I. Skolnik, *Introduction to Radar Systems*, 2nd ed. New York: McGraw-Hill, 1980, ch. 1.

[8] J. M. Kahn and J. R. Barry, "Wireless infrared communications," *Proc. IEEE*, vol. 85, no. 2, pp. 265–298, Feb. 1997.

[9] W.-Y. Shieh, "The analysis of single-lane OBU and RTU optimum setup configuration in automatic electronic-toll-collection systems," Res. Inst. ChungHwa Telecom, Taoyuan, Taiwan, 89-EC-023, Nov. 2000.

[10] ——, "The comparison of the efficacy of two-piece and single-piece RTU LED-module on the down-link data transmission in our ETC system," Res. Inst. ChungHwa Telecom, Taoyuan, Taiwan, 90-EC-001, Jan. 2001.

[11] J. D. Kraus, *Antennas*, 2nd ed. New York: McGraw-Hill, 1988, ch. 3.

[12] *Datasheet of TSHF5400 High Speed IR Emitting Diode in ⌀ 5 mm* $(\mathrm{T}-1(3/4))$ *Package*, Jun. 2003. The Vishay website, 81024.pdf. [Online]. Available: http://www.vishay.com/docs/81024/

[13] *Datasheet of Silicon PIN Photodiode with Daylight Filter*, Mar. 2004. The OSRAM website, bpw34fa.pdf. [Online]. Available: http://www.osram.convergy.de/upload/documents/2004/03/10/15/15/

Lane Detection With Moving Vehicles in the Traffic Scenes

Hsu-Yung Cheng, Bor-Shenn Jeng, Pei-Ting Tseng, and Kuo-Chin Fan

***Abstract*—A lane-detection method aimed at handling moving vehicles in the traffic scenes is proposed in this brief. First, lane marks are extracted based on color information. The extraction of lane-mark colors is designed in a way that is not affected by illumination changes and the proportion of space that vehicles on the road occupy. Next, for vehicles that have the same colors as the lane marks, we utilize size, shape, and motion information to distinguish them from the real lane marks. The mechanism effectively eliminates the influence of passing vehicles when performing lane detection. Finally, pixels in the extracted lane-mark mask are accumulated to find the boundary lines of the lane. The proposed algorithm is able to robustly find the left and right boundary lines of the lane and is not affected by the passing traffic. Experimental results show that the proposed method works well on marked roads in various lighting conditions.**

***Index Terms*—Camera geometry, computer vision, intelligent transportation systems (ITS), intelligent vehicles, lane detection.**

I. INTRODUCTION

In intelligent transportation systems, intelligent vehicles cooperate with smart infrastructure to achieve a safer environment and better traffic conditions [1]. Intelligent vehicles are expected to be able to give route directions, sense objects or pedestrians, prevent impending collisions, or warn drivers of lane departure [2], [3]. Therefore, lane detection is a crucial element for developing intelligent vehicles. Lane detection based on machine vision is accomplished by taking images from cameras mounted on the intelligent vehicles. There are many related research works on this issue in recent years [4]–[17]. These works generally used different strategies aimed at certain kinds of surroundings and road conditions. One category of methods used intensity images as the basis of lane detection. Kluge and Lakshmanan [4] used a deformable template model of lane structure to locate lane boundaries without thresholding the intensity gradient information. Wang *et al.* [5], [6] computed a potential edge field and a potential orientation field image and then applied B-snake or Catmull-Rom spline-based lane model to handle curved roads. Yim and Oh [7] developed a three-feature-based automatic lane-detection algorithm using the starting position, direction, and gray-level value of a lane boundary as features to recognize the lane. Another category of works combined edge information with color information or other features to distinguish the road area from the surroundings. Gibbs and Thomas [8] fused the results of edge detection, road segmentation, and white lane follower to obtain the final detection result. Rasmussen [9] utilized texture features to deal with rural roads that do not have obvious lane marks, under the assumption that the color of road surface is homogeneous. Kluge and coauthor [10], [11] and Gonzalez and Ozguner [12] employed histogram information to select thresholds and detect lane marks. Redmill *et al.* [13] utilized a matched filter and a Kalman filter

Manuscript received July 17, 2005; revised December 9, 2005, June 26, 2006, July 31, 2006, and August 2, 2006. The work of H.-Y. Cheng was supported by the MediaTek Fellowship. The Associate Editor for this paper was L. Vlacic.

H.-Y. Cheng, P.-T. Tseng, and K.-C. Fan are with the Department of Computer Science and Information Engineering, National Central University, Chung-Li, Taiwan, R.O.C. (e-mail: chengsy@fox1.csie.ncu.edu.tw; gf1022@yahoo.com.tw; kcfan@csie.ncu.edu.tw).

B.-S. Jeng is with the Department of Communications Engineering, Yuan-Ze University, Chung-Li 320, Taoyuan, Taiwan, R.O.C. (e-mail: bsjip@cht.com.tw).

Digital Object Identifier 10.1109/TITS.2006.883940